Final Proposal

Aerodynamic & structural analysis of a Kite-Wing, ICARUS

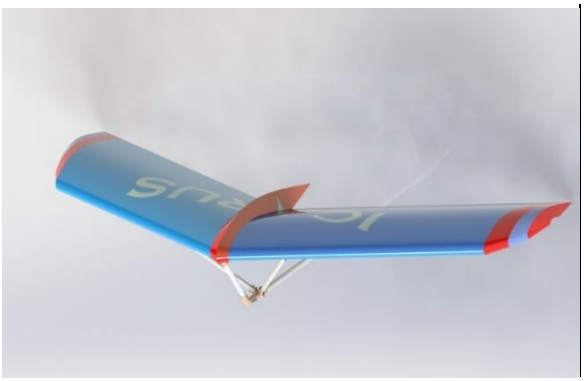

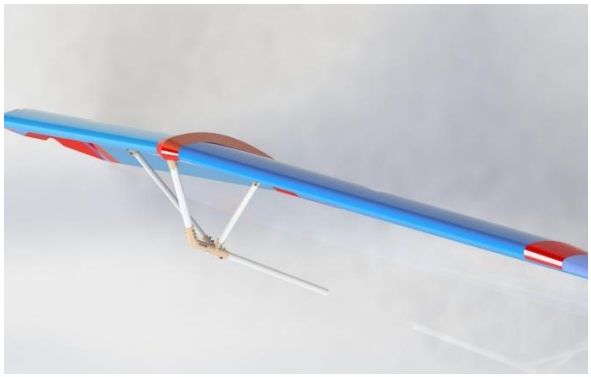

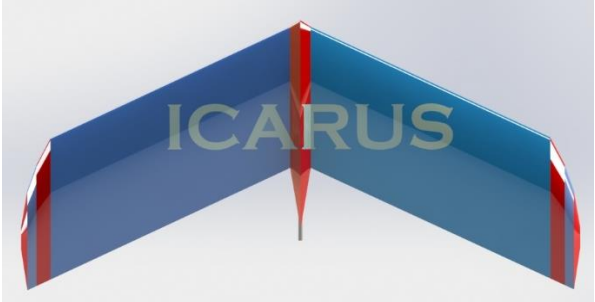

Zidane Moujahidi **April 27, 2017**

Supervisor: Dr.Anas Bentamy

Al Akhwayn University, AUI

Acknowledgment

I would like to express my special thanks and gratitude to Dr.Anas Bentamy, Yassine Khalil, and Hussain. Secondly I would also like to thank my friends who helped me a lot in understanding many aspects of this project by involving in discussions about the presented topic and by trying to simulate the actions and applications.

Contents

Acknowledgment 1

Abstract 4

I- Introduction & Literature Review 4

A- Facts about Kite-Wings 4

B- The Aerodynamics behind Kite-Surfing 6

II- Assessment of the Kite-Wing aerodynamic performance 11

1- Problem Statement 11

2- Pre-analysis and start-up 12

3- Geometry 14

a -Airfoil dimensions 14

b- Wing Dimensions 15

4 - Mesh 16

5- Model Setup 18

6- Numerical Solution 18

7- Numerical Results 19

a- Interpretation of numerical results 19

b- Interpretation of pressure contours, velocity contours, turbulence contours, and 3D- flow around the wing 25

III- Assessment of Kite-Wing's material strength 30

A- Wing Simulation under extreme wind conditions 30

1- Problem statement 30

2- Pre-Analysis & Start-Up 30

3- Geometry 31

4- Mesh 31

5- Model Setup 32

6- Numerical Results 32

B- Stresses and deformations on Sailcloth 34

1- Geometry 35

2- Mesh 35

3- Physics Setup 36

4- Numerical Results 36

C- Strength of the Kite-Wing's frame 38
1- Problem statement 38
2- Geometry 38
3- Physics setup & Solution 42
IV- Conclusion 43
V- Future Work 44
References 44

Abstract

This capstone project is about building a Kite-Wing that is cheap and strong. Also, kite-wings are used to harness the kinetic energy of the wind in order to move in different directions and even to perform long jumps. Moreover, a new design of the Kite-Wing based on aerodynamic principles is provided. Then, the results that are presented in this project are based on investigations on the forces applied on the Kite-Wing, and the resultant material distortions and stresses on it. This research is based on aerodynamic and structural analysis using hand calculations and 3D simulations performed by ANSYS Software. The simulations involve Computational Fluid Dynamics (CFD) and Finite Element method (FEA).

I- Introduction & Literature Review

A- Facts about Kite-Wings

To begin with, Kitesurfing is a new emerging sport which gained popularity, especially, in the last 10 years. Also, it originates from Scandinavia where there are frozen places. And due to the flexibility of Kitesurfing, this sport was brought to Britain and was combined with Dirt-Surf [1]. Basically, a kite-wing is wing sail that is hand held, and it is designed for sailing on surfaces with low coefficients of friction, such as, ice, snow, and pavement. Also, it could be used with skateboards, rollerblades, skates, and skis [2]. Unlike other traditional power kite sports, kite-wings afford greater control and stability, they not have lines that could tangle, and can be manipulated easily to perform diverse tricks, turns and fast speeds [3]. Moreover, learning how to

ride with a kite-wing is fairly easy, and riders who have enough experience can reach speeds up to 90 km/hour and jumps up to 500 meters in inclined surfaces [4].

Then, it is the aerodynamic forces that are applied on the sail of the kite-wing that enable the user to move forward in different directions and different speeds, a more detailed explanation is provided is the subsequent peges. The two images below gives a general idea about the way a kite-wing is used.

Figure 1: Forward motion using a kite-wing

Figure 2: Performance of a long jump

In terms of safety kite-wings are considered to be safe, since they are very maneuverable and close to the user which enable the user to depower instantaneously, in other words, reducing velocity by directing facing the kite-wing toward the wind. However, safety cautions are necessary, such as, wearing a helmet, knee and elbow pads. In addition, choosing the size of kite-wing is based on the weight in order for the rider to have a better control and maneuverability [5].

Furthermore, kite-wings are produced by one company in the world in Finland, and they are very expensive. Then, their price ranges between 749 $ and 1,899 $ which means that not everybody can buy one [6]. Their expensive price is explained by the fact that the frame of the

kite-wings is made of carbon fiber and Dacron sailcloth [7]. Hence, attempting to build a Kite-Wing that is performant, cheap, strong, is desirable in order to make it more accessible to people who want to practice kite-surfing and in order to remove constraints that are facing the growth and development of this sport.

B- The Aerodynamics behind Kite-Surfing

The aerodynamic forces will be explained referring to the following figure:

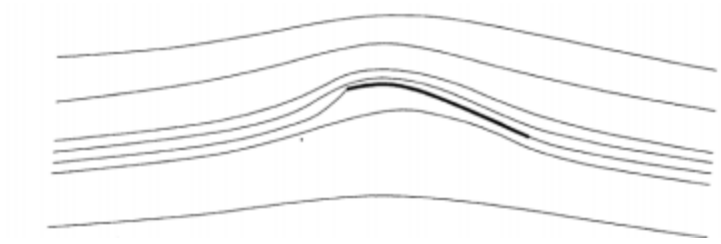

Figure 3: Flow arround a sail

Figure 3 represents a sail being subject to airflow and which has two sides the leeward (above) side and the windward (below) side. Since the sail is cambered, the air particles on the leeward size move faster compared to the air particles moving on the windward side [8]. According to Bernoulli's principle, when the air particles move fast the pressure is low and when the air particles move slowly the pressure, therefore, a suction on the leeward sail is created which is in turn responsible for the generation of aerodynamic forces [9].

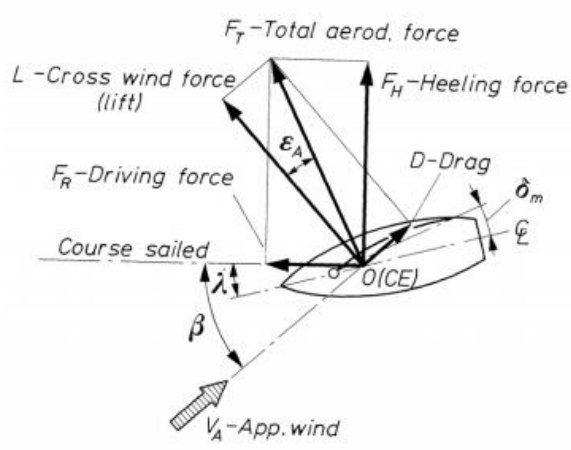

Figure 4: Generation of lift ,drag, thrust and heeling forces.

Figure 4 shows that the aerodynamic force is composed of two vectors, one representing the drag force (D) which is always in the direction of the wind, while the second vector represents the lift force (L) which is always perpendicular to the drag force [10]. It is also important to mention that the lift force and the drag force are dependent on the angle of attack (α), and that the lift force is predominant as long as it is under a critical angle of attack, otherwise, a flow of separation is created causing the drag force to become dominant[11].

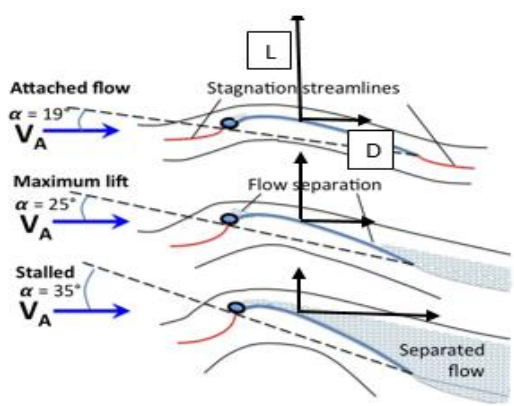

Figure 5: Generation of lift and drag force with respect a varying angle of attack

Furthermore, when traveling in upwind direction the drag force is considered as an undesired force. Also, experiments and theories assert that the drag force is composed of the induced drag, skin friction drag, and pressure drag [12]. The induced drag or tip vortices are caused by the pressure difference on the leeward and windward sides near the edges of a sail or a wing. Moreover, it is quantified using the following formula [13].

$C_{Di} = {C_L}^2/A * \pi$ And $A = \mathrm{b}^2/S$

Where

C_L =Lift coefficient
A =Aspect ratio
b= length of the sail
S = sail area

Also, the rotating mass of air (vortices) behind the sail creates a loss of wind kinetic energy. The induced drag can be reduced in many ways, among them is to use elliptical wing shape [14]. The following figure depicts the induced drag phenomena

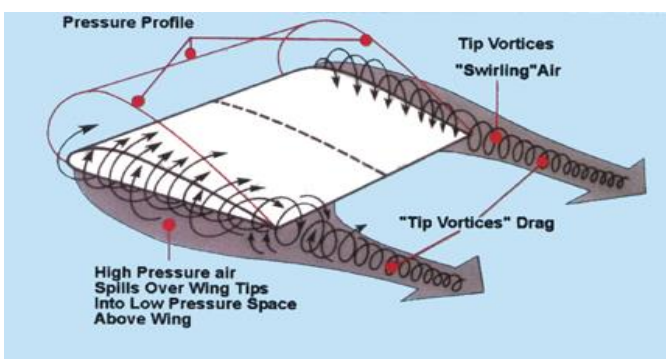

Figure 6:Induced drag phenomena

While the friction drag is due to the shear stresses caused by the viscosity of air at the boundary layer. And its effect is considered to be small [15].

Concerning the pressure drag, it arises from the form of the sail. Generally, the more it is curved the more regions of flow separation will be created [16].

In addition, the aerodynamic principles behind sails are the same as kite-wings. In the following lines other forces shall be introduced, the thrust force F_R and the heeling force F_H. The thrust force is the one responsible moving a given load forward while the heeling force which is the lateral force acting on the sail. These two forces are dependent on the lift, drag and angle between the wind and the course of the sail or kite-wing. Also they are related by the following simple trigonometric equations [17].

$$F_R = L\sin\beta - D\cos\beta$$
$$F_H = L\cos\beta + D\sin\beta$$

It is observed from these two equations that the aim when sailing is to increase the thrust force and decrease the heeling force in the same time. And for this to happen, the lift to drag ratio should be high as possible at a given angle (β).

Moreover, the angle (β) changes with the point of sail. Basically the point of sail the related to the course or direction of the boat with respect to the upwind or the downwind ,and the following figure shows different positions where each one of them has a specific name.

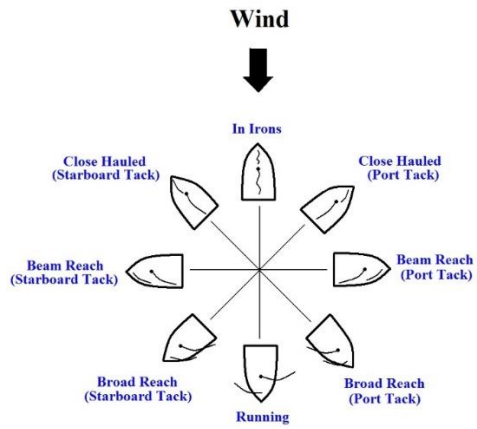

Figure 7: Point of sail

In figure 7, it is noticed that the only position where the load does not move forward is in iron position, and this is because the sail is not directed with an appropriate angle of attack, hence, no lift and thrust is generated at this point of sail [18].

Usually when sailing or riding a kite-wing it is not only the true with that is involved but also the speed of the load giving rise an apparent wind speed which is the speed seen by the sail or the kite-wing [19]. The following figure illustrates this phenomena

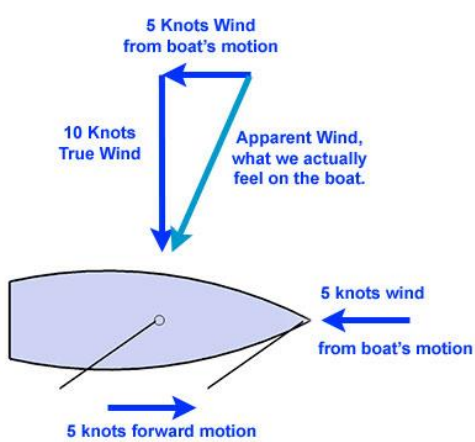

Figure 8: Apparent wind speed

II- Assessment of the Kite-Wing aerodynamic performance

In order to assess the performance of the Kite-Wing, CFD (Computational Fluid Dynamics) simulations were performed using ANSYS fluent software. It worth mentioning that CFD simulations enable a better visualization the flow around objects. In this project, pressure contours, velocity contours, and turbulence contours were generated and described concisely. Also, coefficient, such as, the lift and drag coefficient were generated in order to determine the performance of the wing under different scenarios. The following steps were performed in order to achieve a CFD Analysis.

- Problem statement
- Pre-Analysis & Start-Up
- Geometry
- Mesh
- Model Setup
- Numerical Solution
- Numerical Results

1- Problem Statement

In order to determine the performance of the Kite-Wing, aerodynamic forces, such as, the lift and the drag should be determined under a specific wind speed and different angles of attacks. The relative wind speed that is chosen for this study is 10 m/s where the angles of attacks are 10°,15°,18°,20°,30°,and 35°. Also, it is important to mention that the Reynolds number is

$Re = (rho*l*v)/\mu$ = (1.22∗1.10∗10)/ 1.78∗10^-5 = 753932.58

Where

Rho: Air density $\frac{kg}{m^3}$

L: Chord length (m)

V: Velocity (m/s)

Since the Reynolds number is greater than 4000, then, the flow is turbulent. Also, the flow was assumed to be steady.

2- Pre-analysis and start-up

This CFD simulation is governed by the continuity, energy equations and Navier-Stokes (conservation of momentum), and because flow is turbulent the Reynolds Averaged version of these equations was used. Moreover, in order to solve the RANS (Reynolds-averaged Navier-stokes equation) SST-Kw (Shear-Stress-Transport) model was used. It is worth mentioning that according to sharcnet website the SST-Kw was designed to provide accurate predictions of flow separations that are subject to adverse pressure gradients [20] .This later was done by including transport effects into the formulation of the eddy-viscosity. Also, this model and according to Bardina et al has been demonstrated in many validation [21].

In addition the flow domain is bounded by boundary conditions, the table below summarizes the boundary name, boundary type and boundary condition, and it is followed by figure 9 which illustrates the boundary conditions.

Boundary name	Boundary type	Boundary condition
Wing Surface	**Wall**	**V= 0 m/s**
Inlet	**Inlet-velocity**	**V=8 m/s, Z and Y Components change with each angle of attack Pressure= 0 Pa**
Outlet	**Outlet-pressure**	**Pressure= 0 Pa**
Symmetry	**Symmetry**	**Boundary**

Table1: Boundary name, boundary type and boundary condition

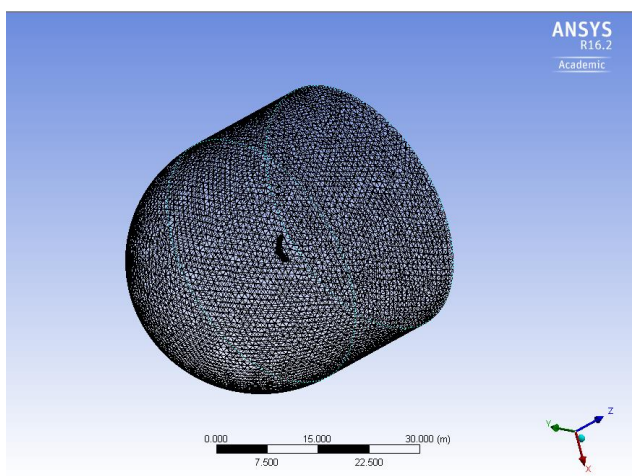

Figure 9: Flow domain boundaries

Where the inlet is the at dome shape surface, the outlet is the circular area at the end of the flow domain, and the symmetry region is the cylindrical region surrounding the wing surface which is in the middle of the flow domain.

3- Geometry

a -Airfoil dimensions

Designing the Kite-Wing starts from choosing an appropriate airfoil which will determine the overall performance of the wing. According to Matthew R. Avila current shapes have less camber with the maximum camber point closer to the mid-cord [22]. Less cambered airfoil means that less turbulences will be under the convex shape of the airfoil, hence, the sail will experience less drag forces and better wing performance. Based on these information the airfoil was designed. The following table 2 and figure 10 represents the airfoil characteristics.

Airfoil Characteristics	**Values**
Chord length	1.10 m
Maximum camber	0.12 m
Camber ratio	11.27%

Table 2: Airfoil characteristics

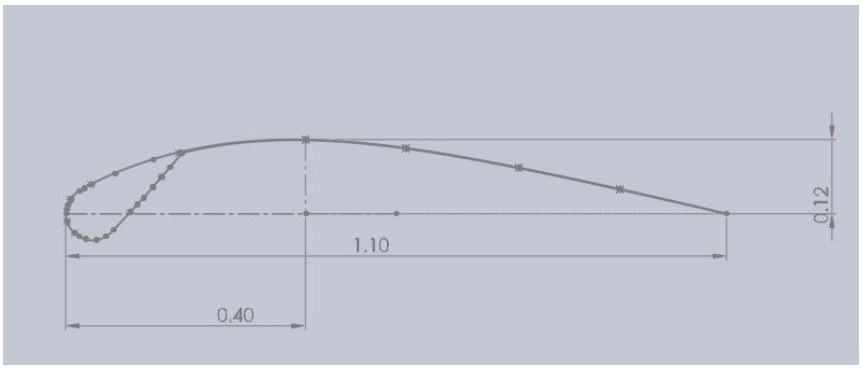

Figure 10: 2D drawing of an Airfoil

It should be noticed that the leading edge of the airfoil had a circular shape which conforms the shape of bars.

b- Wing Dimensions

After choosing and drawing the airfoil, the next step is the model the 3D wing. To do so, airfoils of different chord lengths were drawn in different planes and then joined together in CAD software (SolidWorks). According to Sigbard Hoerner, rounded edges wings facilitate the flow around wings, and they can reduce the effect of the induced drag [23]. And according to Steve Garber high aspect ratio wings increase the lift to drag ratio [24]. Hence, these advantageous characteristics were taken into account into the current wing design.

Wing Characteristics	**Values**
Wing Span	4.34 m
Planar Area	4.74 m^2
Sweep Angle	65°
Aspect Ratio	3.97

Table 3: Wing dimensions

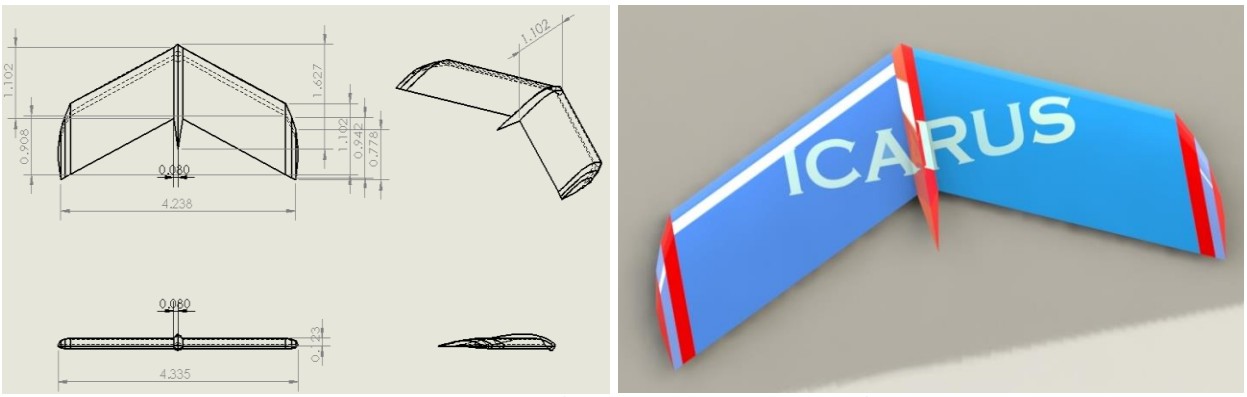

Figure 10: 2D drawing of the Wing & 3D model of the Wing

In addition, the wing is swept because it will enable a better maneuverability and stability, especially, in short flying distances.

After modeling the wing in CAD (SolidWorks) as described previously, it was imported to ANSYS design molder as an IGES file, then, a flow domain which a has a C-Shape was created around the wing in ANSYS design modeler. The total volume is large enough, and this is because flow should be captured very well around the wing.

4- Mesh

In order to determine the aerodynamic properties of the wing, separation bubble, and the flow the mesh should be fine to capture the flow around the wing and the forces on it. To achieve this, a fine tetrahedron-mesh was chosen and the size function was applied on the wing surface resulting 0.01 m element sizes on wing surface. Also, an inflation layer was created around the wing in order to capture the changes of the velocity gradients which highly affect the lift and drag coefficients. In addition, the total thickness can only be approximated by using the following formula: $Del(y) = \frac{0.38*x}{(Re,x)^{1/5}} = \frac{0.38*1.10}{(753932.58)^{1/5}}$ = 0.0279m

Where

Re: Reynolds Number

X: Chord length (m)

Also, according to leap team it is a good practice to use a number of 10 to 15 inflation layers [23], since it offers a better flow resolution near the wing. In this simulation 15 inflation layers were used. At the end of the meshing step, a mesh with the following characteristics was obtained:

Number of nodes	**Number of element**	**Maximum skewedness**	**Minimum Orthogonal quality**
2110073	6240339	0.99998	3.5099e-003

Table 4: Mesh characteristics

It should be noted that the maximum skewedness is high and orthogonal quality is low which criteria of a bad mesh quality, and this is due to the highly curved and edged wing model. However, the number of these bad element is statistically very small as figure 11 illustrate.

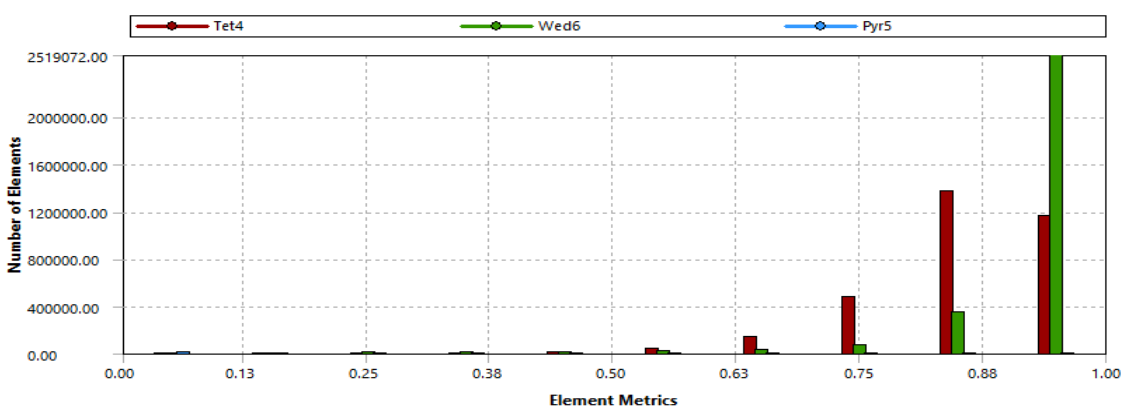

(a)

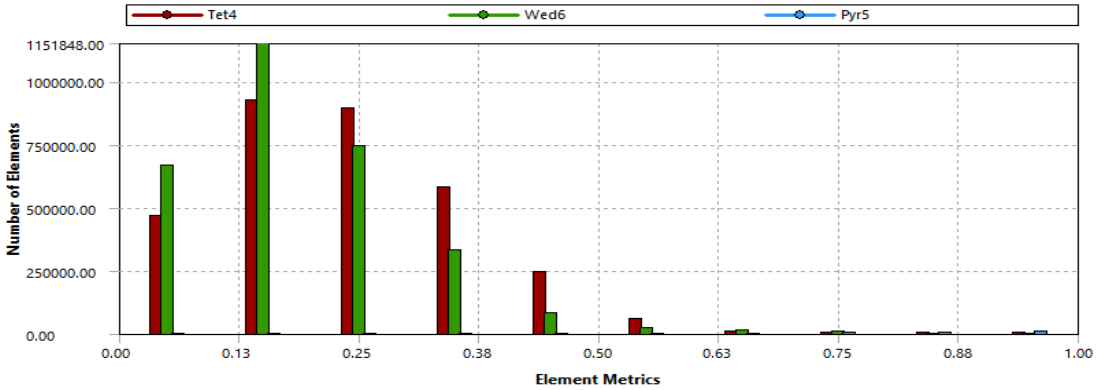

(b)

Figure11: Mesh quality a) Orthogonal quality vs. number of elements b) Skewedness vs. number of elements

5- Model Setup

At this stage, the SST-kw was set besides the boundary conditions and the air density was set to be a constant, which implies an incompressible flow. Attention should be paid here, since the angle of attack changes after each simulation the Y and Z components change as well. For instance, when the velocity is 10 m/s and the angle of attack is 18° Y-Velocity= $10 * (18) = 3.090$ m/s and Z= $10 * (18) = 9.510$ m/s.

6- Numerical Solution

The solution method that was chosen for this simulation is coupled, pseudo transient, and high order relaxation. Coupled is pressure-based coupled algorithm which is robust and efficient single phase implementation for steady flows. Where pseudo transient and high order relaxation are options that help in the convergence of the solution. Also the convergence criteria was set at 10^3

7- Numerical Results

a- Interpretation of numerical results

After simulating the airflow around the wing at 10m/s and different angles of attack 10°, 15°, 18°, 20°, 30°, and 35° respectively the following results were obtained.

Angles of attack	**Cl**	**Cd**	**Cl/Cd**
10°	2.641	0.621	4.252
15°	3.309	0.912	3.626
18°	3.678	1.135	3.239
20°	3.974	1.306	3.042
30°	6.271	2.513	2.495
35°	6.569	2.943	2.231

Table 5: Values of Cl, Cd, and Cl/Cd at different angles of attack

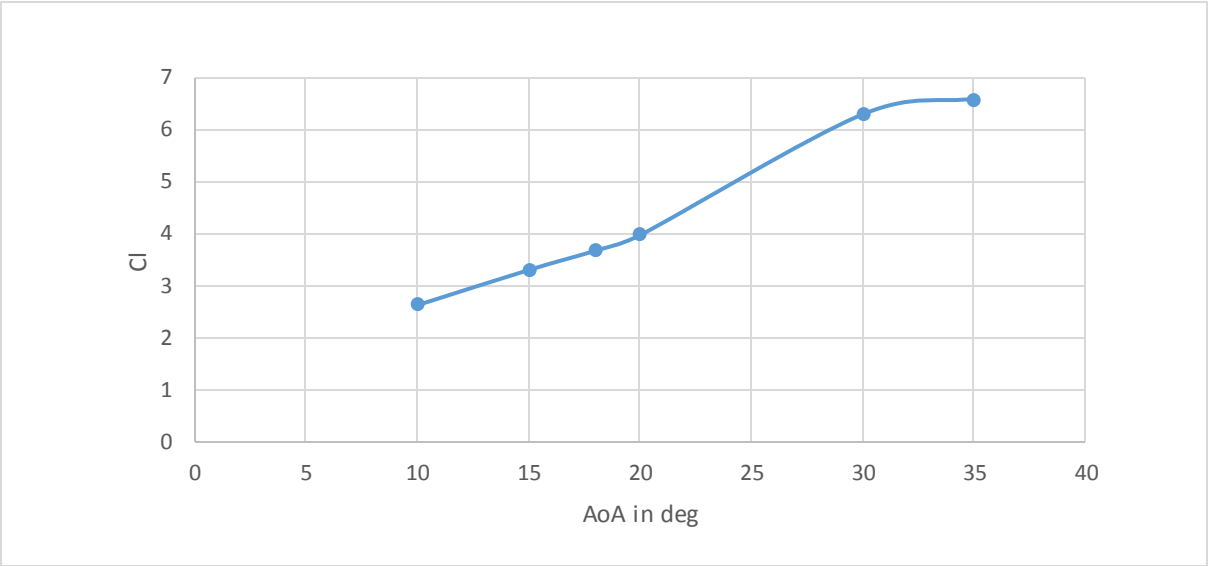

Graph 1: Lift Coefficient vs. Angle of Attack

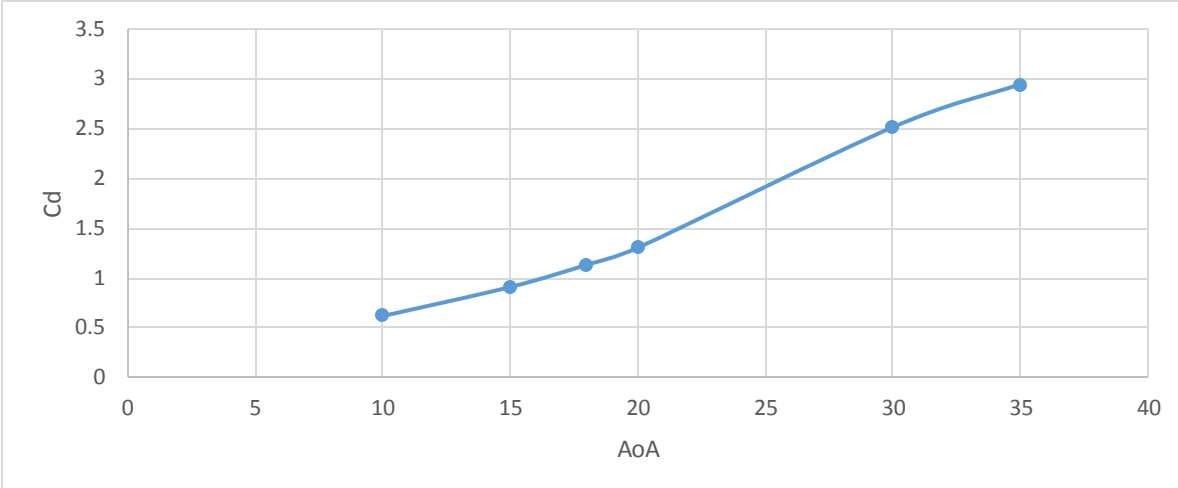

Graph 2: Drag Coefficient vs. Angle of Attack

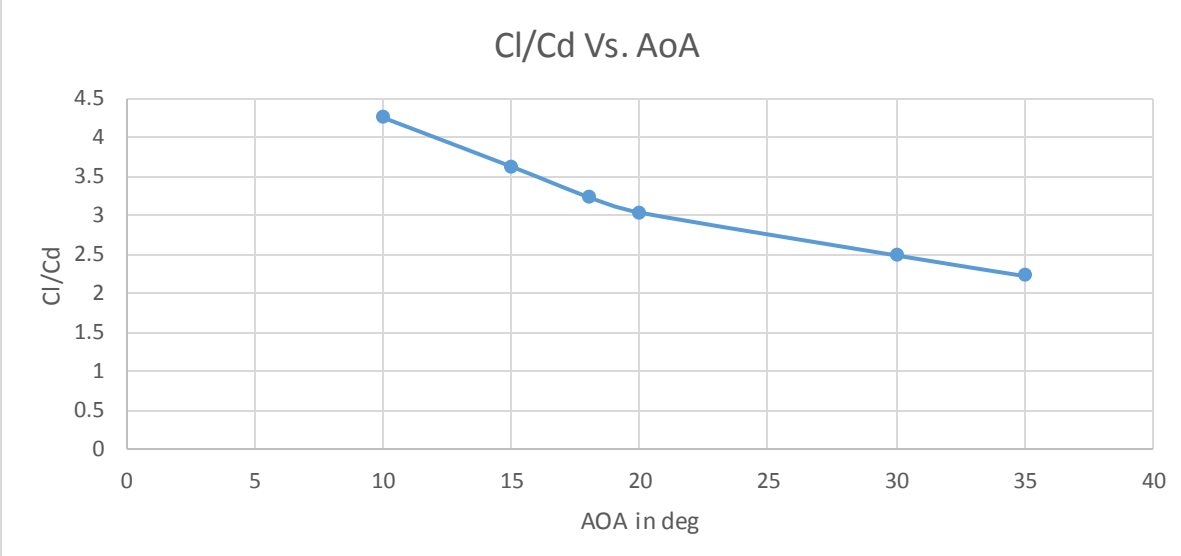

Graph 3: Lift to drag ratio vs. Angle of Attack

The results show that the lift and drag coefficients are high, and this could be explained by tear-drop shape of the airfoil and the high Reynolds number. Also, it is noticed that as the angle of attack increases the lift and drag coefficient increase as well. In graph 1, the lift coefficient starts at a value of 2.641 when AoA is 10°, then, it keeps increasing up to a value of 6.271 when AoA is 30° then it increases with a very small value up to a value of 6.569.

While for the drag coefficient, graph 2 shows that it starts at 0.621 when AoA is 10° which a small value relatively to the lift coefficient. Then, it keeps increasing up to a value of 2.513 when AoA is 30° and increases to 2.943 when AoA 35°. It is noticed that both the lift and drag coefficients increase with very small values between 30° and 35°.

Concerning the lift to drag ratio, it appears from graph 3 that the highest value is 4.252 when AoA is 10°, and this means that the lift is dominant compared to the drag. Also, as the AoA increases the lift to drag ratio decreases down to a value of 2.231 at an AoA of 35°, and this implies that the value of the drag coefficient is getting closer to the lift coefficient. Yet, it is clear that at all the angles of attack the lift coefficient is always higher than the drag coefficient.

Before starting in the description of the flow around the wing, it is worth restating the conditions at which the wing is simulated. The airflow is steady, incompressible and turbulent, also, the velocity is 10 m/s and the angles of attack under which the wing simulated are 10°, 15°, 18°, 20°, 30°, and 35° respectively. The following figures, namely, 12.a, 12.b, and 12.c include groupings of figures of velocity contours, pressure contours and turbulent contours under aforementioned scenarios. It is emphasized that the following figures were taken in the YZ plane and 1 m from the symmetry plane of the wing.

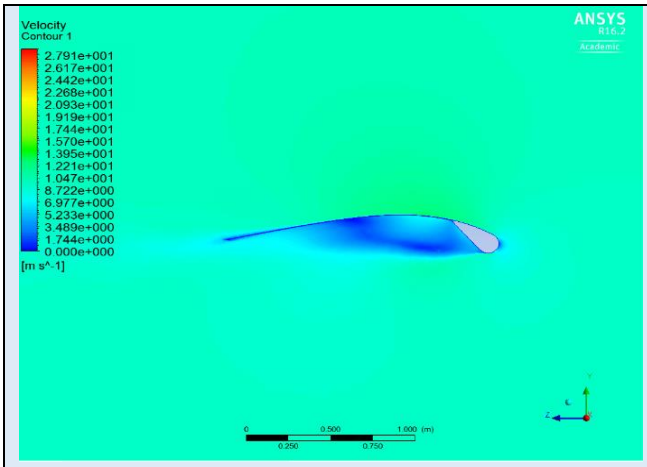

AoA=10°

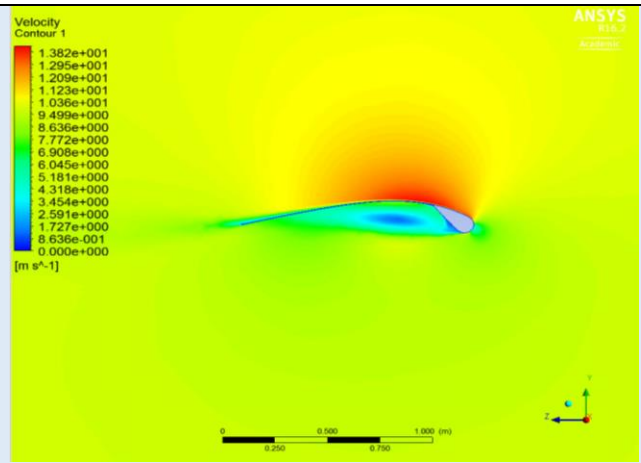

AoA=15°

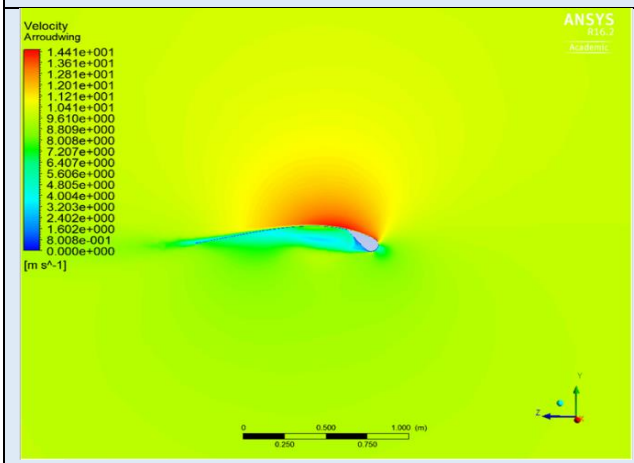

AoA=18°

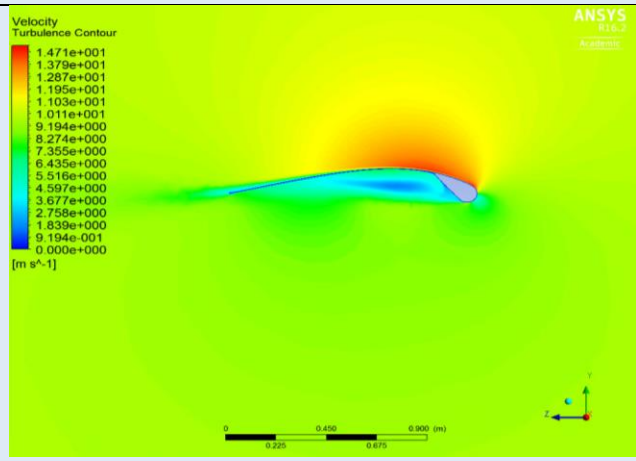

AoA=20°

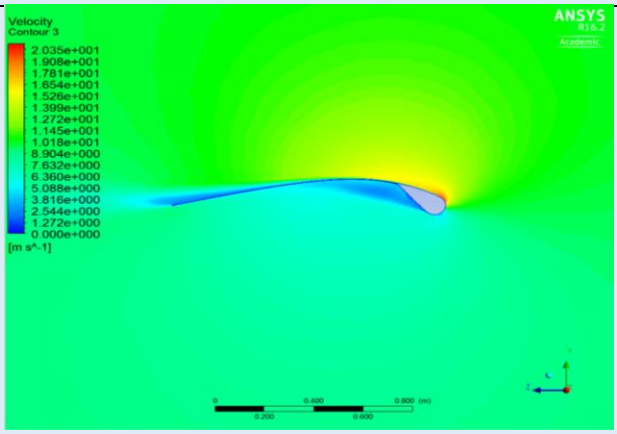

AoA=30°

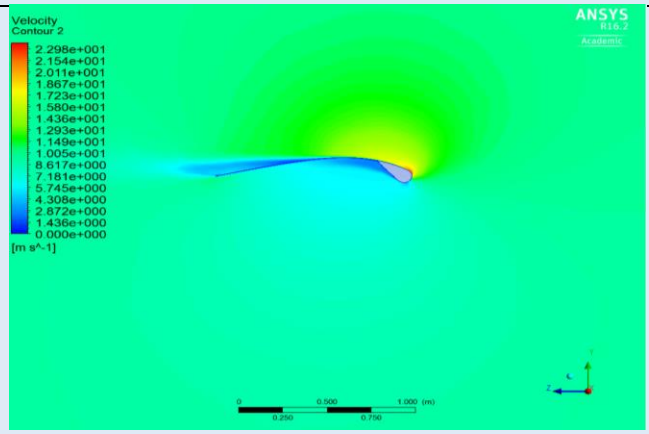

AoA=35°

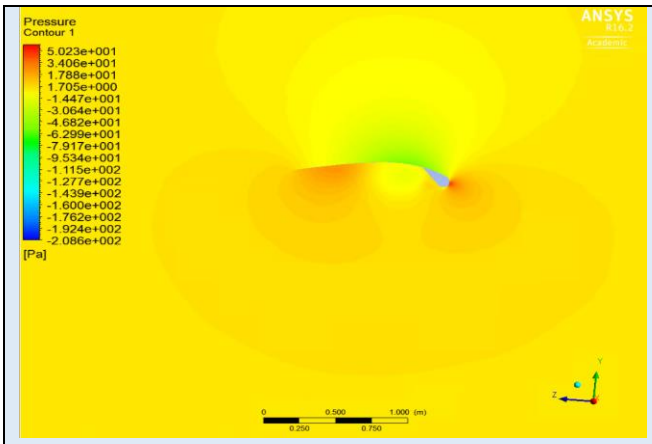

AoA=10°

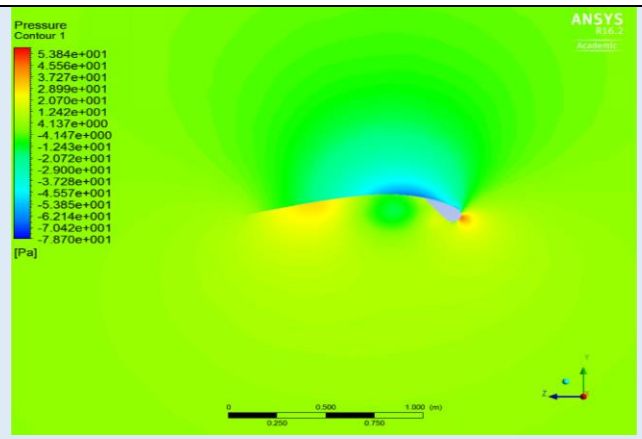

AoA=15°

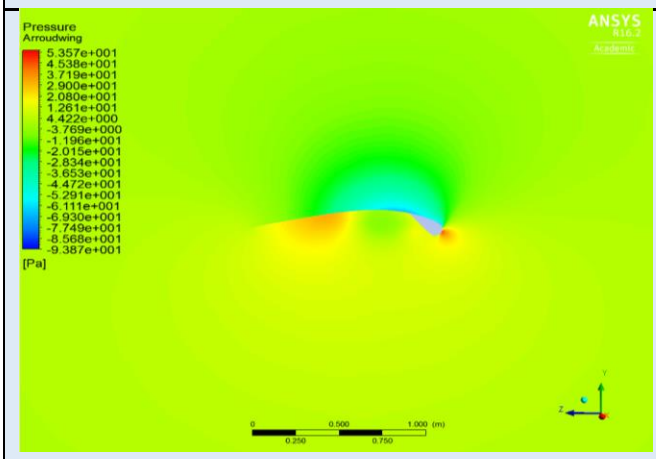

AoA=18°

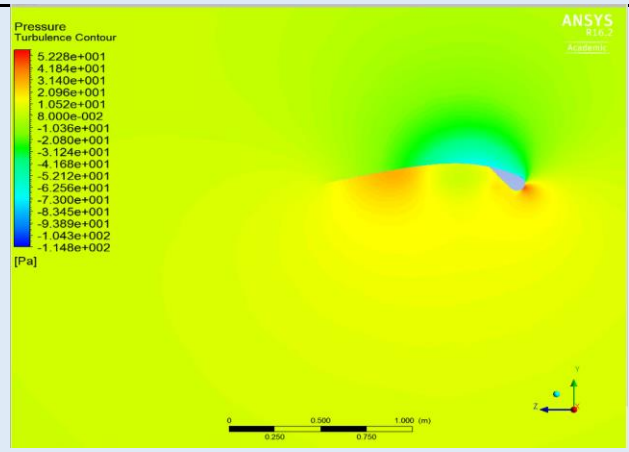

AoA=20°

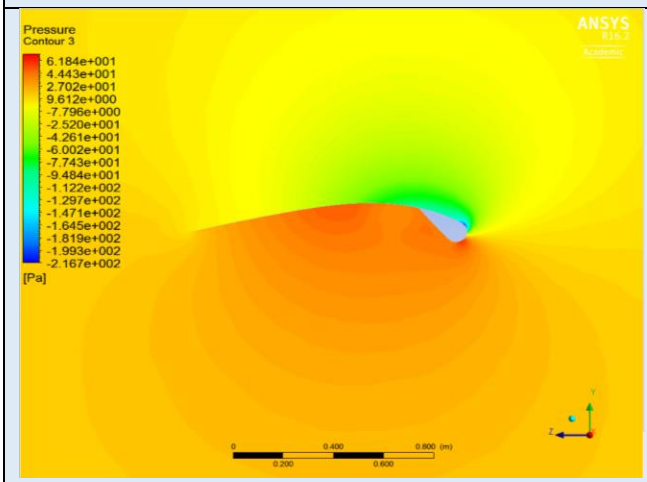

AoA=30°

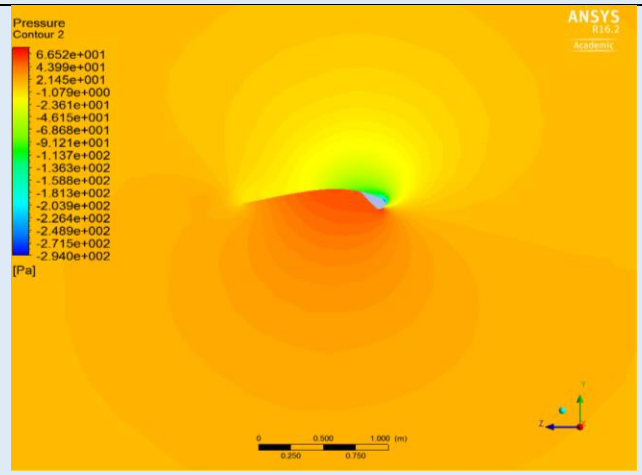

AoA=35°

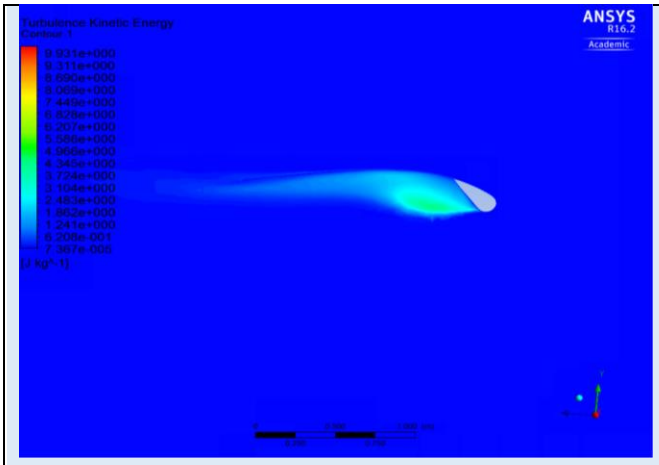

AoA=10°

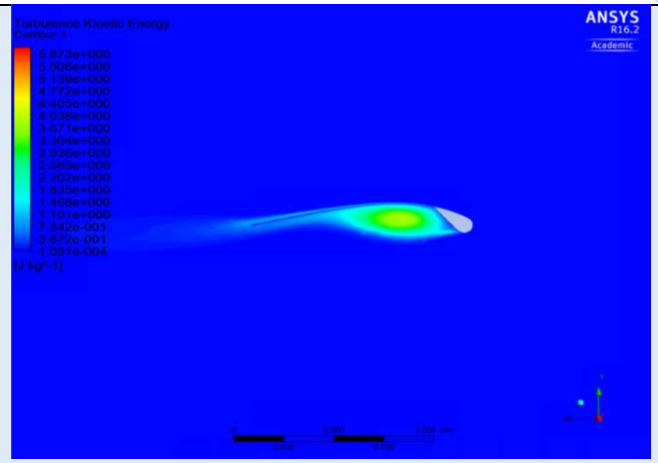

AoA=15°

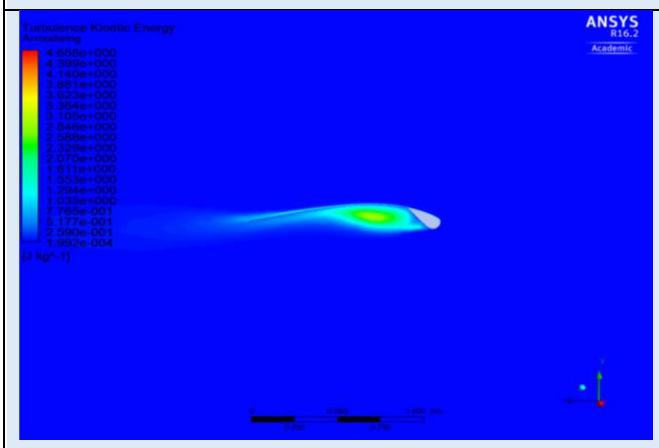

AoA=18°

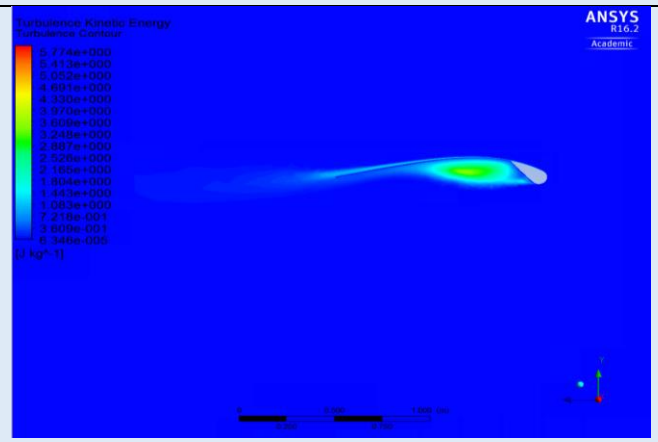

AoA=20°

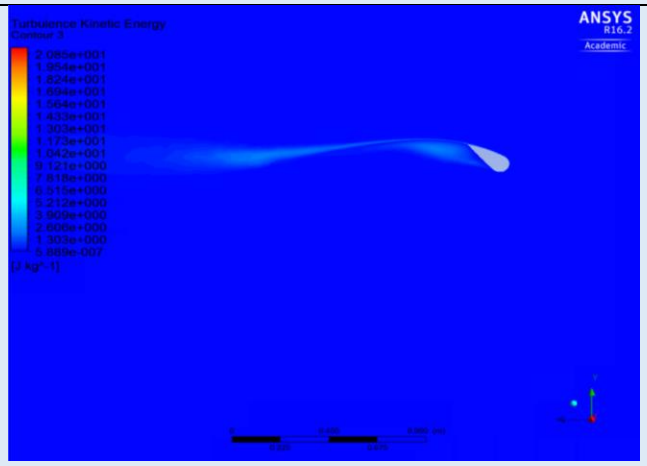

AoA=30°

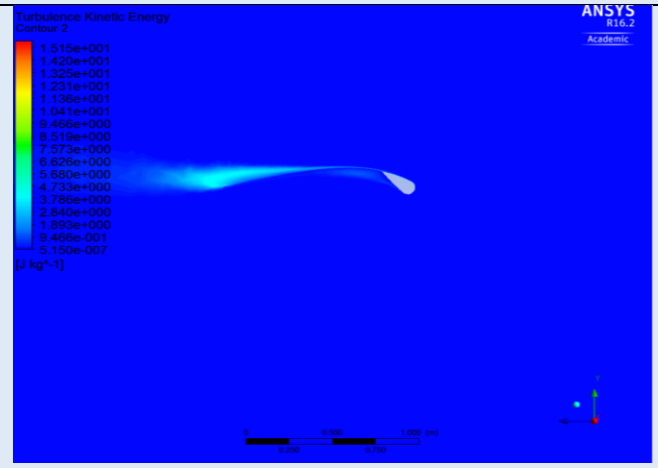

AoA=35°

Figure12: a) Velocity contours grouping b) Pressure contours grouping c) Kinetic turbulent energy contours grouping

b- Interpretation of pressure contours, velocity contours, turbulence contours, and 3D-flow around the wing.

Since the flow characteristics, meaning, velocity, pressure, and turbulence are all dependent on each other a concise description of the flow shall be dealt with in the following lines.

To start with, the air flow that is approaching the wing is irrotational, and its kinetic energy is in the form of linear velocity.

Then, when the flow hit the leading edge the stagnation point forms, meaning, the airflow comes to a halt leading to a high pressure indicated by the red region which changes location as the angle of attack in increased from 10° to 35°, and this is illustrated in the pressure contours.

As the flow moves forward it gets divided into two regions one below the wing the other above it, where the two regions have different pressures and velocities.

According to Bernoulli's equation, there is an inverse relationship between the static pressure and the velocity. When the local pressure is negative (blue/white region) this means that it is less than the atmospheric pressure, and that the velocity is higher than the velocity of the airflow around the wing. Positive local pressure (red region) implies that the velocity is lower than airflow around the wing. For instance, at an AoA of 30° the pressure under the wing reaches 61.84 Pa where the velocity is almost 0 m/s. But at the top surface of the wing the pressure is -150 Pa, and the velocity is approximately 15 m/s. Also, it is this pressure difference that creates a normal force which is the lift force.

Concerning the turbulences, at low AoA , meaning, between 0° and 20° the turbulences are found to be under the convex region of the wing and the corresponding to a range of turbulent kinetic energy between . This happens because of the shape and sharpness of the leading edge, as the air flow approaches the leading edge a laminar separation, meaning that the flow becomes turbulent ending up by creating a turbulent boundary layer. Moreover, in the mid-section of the airfoil the kinetic turbulent energy reaches 8.096 J/Kg, this happens mainly because we have a circulating flow under the convex region of the wing. As the air flow continues to flow the turbulent reattachment happens followed by a turbulent boundary layer behind the trailing edge. It should be noted that the separation bubble where the air flow is recirculating extends between the laminar separation and the turbulent reattachment.

Furthermore, when the AoA is higher than 20° the separation almost bubble disappears, nevertheless, it is substituted by low turbulences at the trailing edge.

After describing the air flow around using the previous two dimensional figures. Now 3D flow characteristics shall be dealt with. The 3D air flow shall be described when the wing is subject to 10 m/s at an AoA of 30°.

One of the most important characteristics of 3D air flow are vortices which occur that the tips of the wing. As the air is free to move at the wing tips, and as there is a difference in pressure between the windward and leeward sides of the wing the resulting flow is in the form of vortices as shown in figure 14.

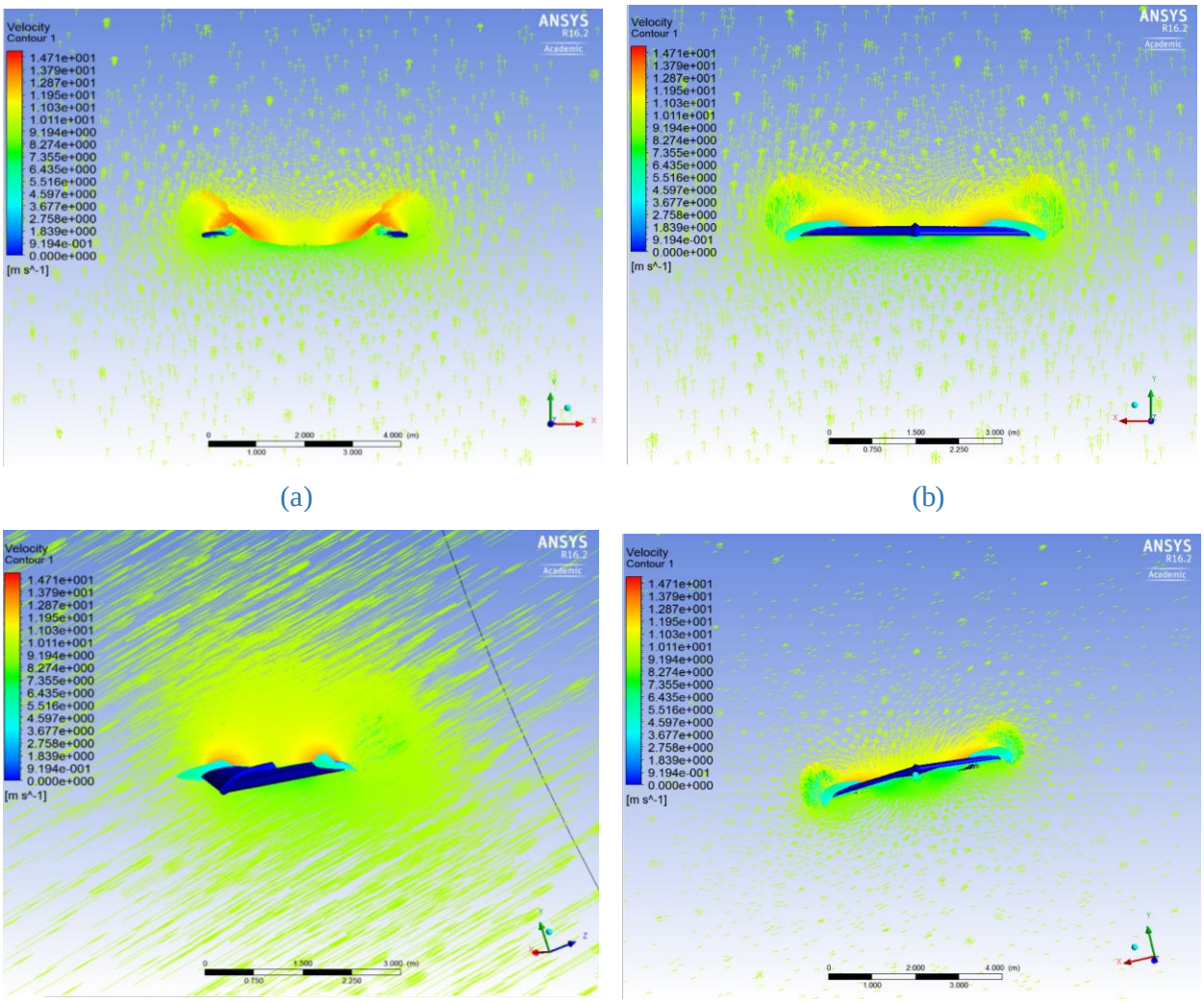

(a) (b)

(c) (d)

Figure 15: Velocity vectors around the wing and velocity contours on the wing a) Rear view b) Front view c & d) Side views

Figure 14 shows the vortices that are created when the air flow travels around the wing from different perspectives. Also, when the air flow hits the wing the velocity decreases in the front side decreases, but as soon as the air flow reaches the ends of the wing tips the airflow gains speed, 14.7 m/s, exceeding the velocity of the inlet, that is, 10 m/s .Moreover, as the angle of attack increases the lift-induced drag increases resulting in a downward force acting at the top of the,

therefore, decreasing the wing performance. Besides this, the flow velocity is 0 m/s at the surface of the wing, and this is known as the no-lip condition.

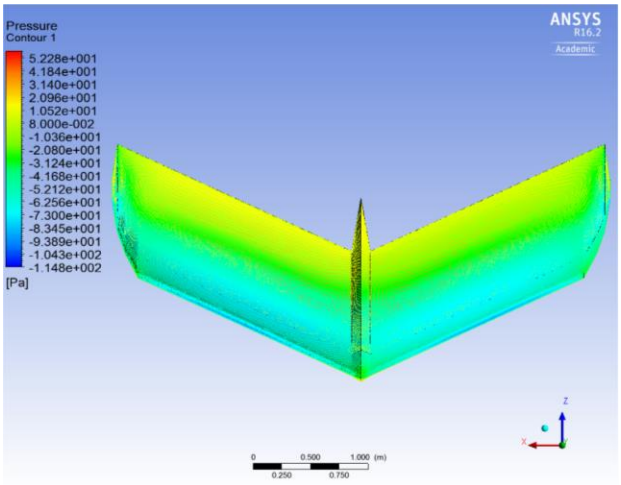

(a)

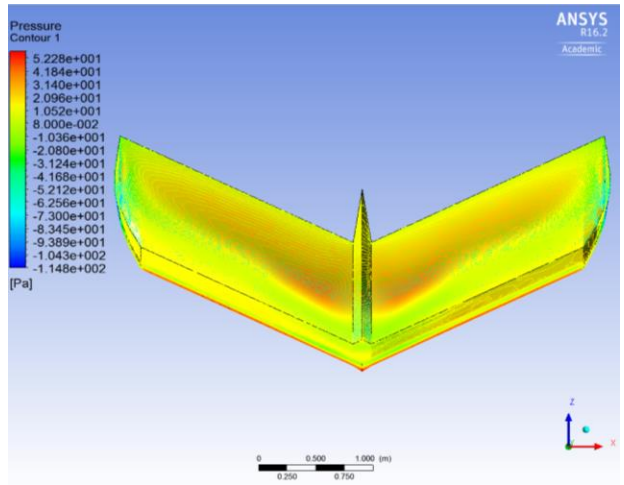

(c)

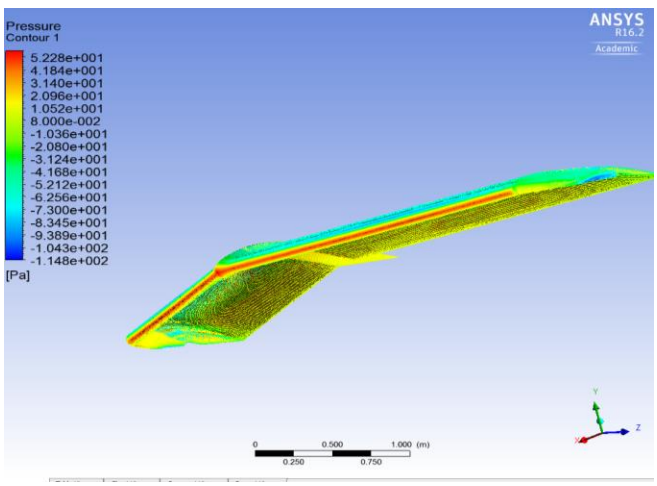

(d)

Figure 16: Pressure contours on the 3D wing a) Top View b) Bottom view c) Isometric view

From figure15, it is noticed that the highest pressure is at the leading edge precisely at the stagnation point where the velocity is 0 m/s. Also the pressure under is around 50 Pa. Where at the top surface the pressure is low around -104.8 Pa

As the wing lift and drag coefficients were found using ANSYS software, the reader may want know the lift and drag forces that are generated in the previous scenarios, hence, the following table is provided.

Angle of Attack	**Drag Force (N)**	**Lift Force (N)**
10°	38.053	161.815
15°	55.907	202.72
18°	66.803	216.417
20°	80.004	243.415
30°	147.856	368.978
35°	180.315	402.385

Table 6: Angle of attack and the corresponding drag and lift forces

It is clear from the previous table that the lift force is always greater that the drag force, and that both of the forces keep increasing linearly as the angle of attack increases. Also, the lift and drag forces are related for the thrust and heel forces by the following relationship:

$$F_R = L\sin\beta - D\cos\beta$$
$$F_H = L\cos\beta + D\sin\beta$$

The angle beta was taken to be 90° in order to maximize the thrust force (propulsive force), and the results are provided in the following table.

Angle of Attack	**Thrust force(at 90) (N)**	**Heeling force (at 90) (N)**
10°	161.815	38.053
15°	202.72	55.907
18°	216.417	66.803
20°	243.415	80.004
25°	368.978	147.856
35°	402.385	180.315

Table 7: Angles of attacks and the corresponding thrust and heeling force

III- Assessment of Kite-Wing's material strength

A- Wing Simulation under extreme wind conditions

After the determining the wing performance at 10 m/s and at different angles of attacks, the frame strength was assessed by using Computational fluid dynamics and Finite element method. The first part deals with CFD analysis, and the following steps were followed:

- Problem statement
- Geometry
- Mesh
- Model Setup
- Numerical Results

1- Problem statement

In order to assess the strength of the frame, it had to be generated under extreme wind conditions. In this case the wing velocity was 20 m/s normal to the wing. Also, the flow is considered to be steady, incompressible, and turbulent. And the flow is turbulent because the Reynolds number is high and the wing constitutes a bluff body in front of the flow.

2- Pre-Analysis & Start-Up

The pre-analysis & Start-Up part is the same as the one stated in the wing performance part except that the velocity inlet is 20 m/s

3- Geometry

The geometry is the same as the one stated in the wing performance part. However, the flow domain is larger this time because it was expected that there will be lots of turbulences behind the wing.

4- Mesh

The mesh that was used in this case has a fine relevance center and the face size function was applied on the wing surface resulting in 0.01 m element size. This was done in order to capture the airflow concisely.

Number of nodes	Number of element	Maximum skewedness	Minimum Orthogonal quality
2110073	6240339	0.999	3.40e-3

Table 6: Mesh characteristics

It should be noted that the maximum skewedness is high and orthogonal quality is low which criteria of a bad mesh quality, and this is due to the highly curved and edged wing model. However, the number of these bad element is statistically very small as figure illustrate.

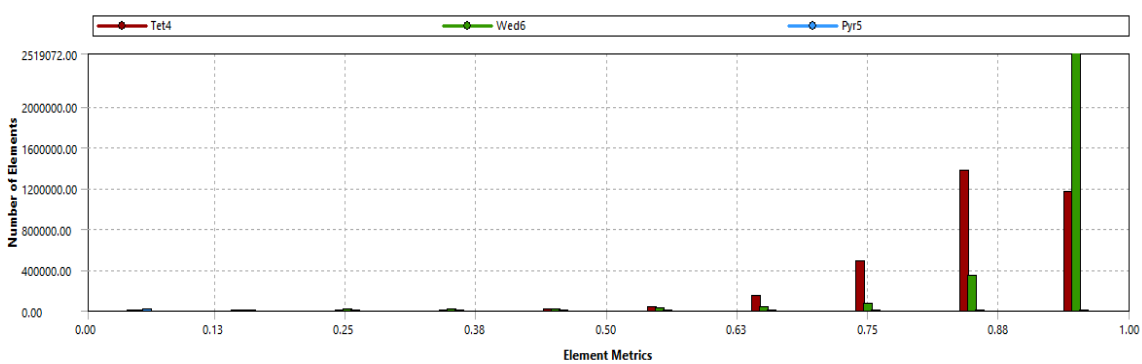

(a)

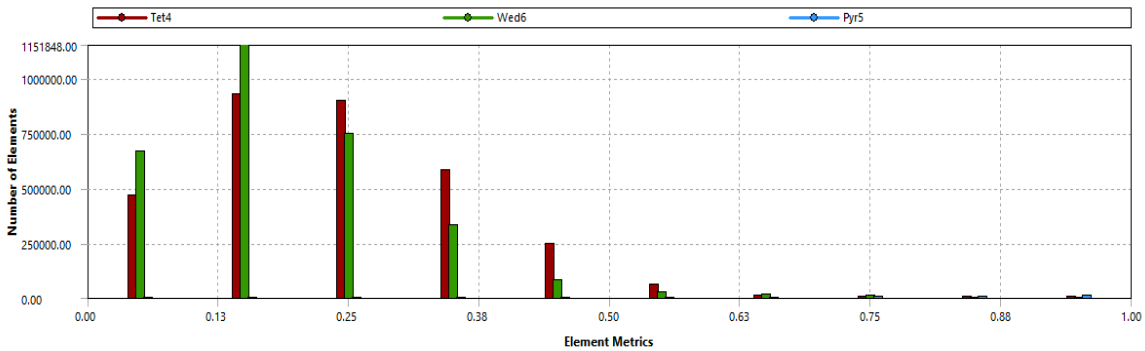

(b)

Figure 17: a) Orthogonal quality vs. number of elements b) Skewedness vs. number of elements

5- Model Setup

At this stage, the SST-kw was set besides the boundary conditions and the air density was set to be a constant, which implies an incompressible flow. And the velocity is 20 m/s at inlet in the positive z-axis.

6- Numerical Results

At this stage of the analysis pressure contours, velocity contours, turbulence contours and the force exerted on the wing are provided and described thoroughly. Also, these contours were taken at yz-plane and 1 m away from the symmetry plane.

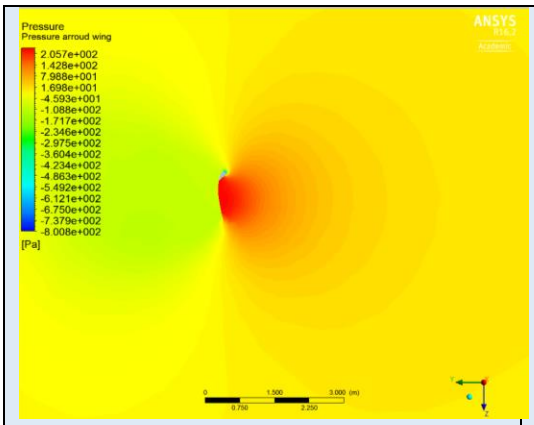

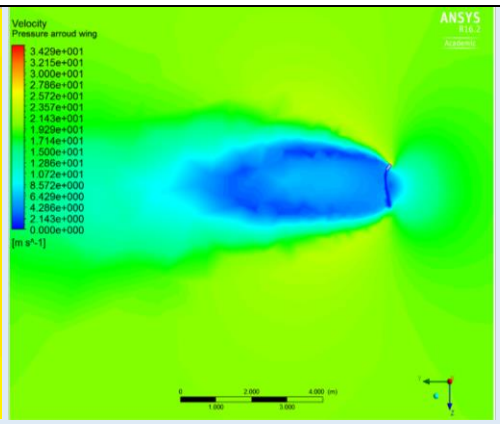

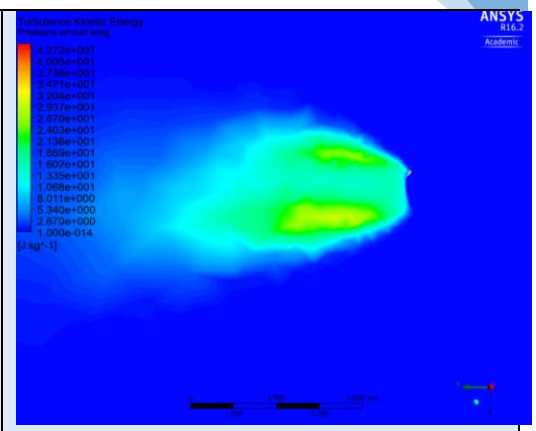

Pressure contours	Velocity contours	Turbulent contours

Figure 18: Pressure contours, velocity contours, and turbulent contours

As it is seen from table, the wing constitute a bluff body in front of the air flow, and the pressure is very high at the convex region of the wing and reaches a value 205.7 Pa. The velocity contours show that the velocity behind the wing becomes 0 m/s. Also, the flow becomes very turbulent behind the wing where the turbulent kinetic energy is around 23.0 J/Kg. It should be also reminded that this case is dominated by the drag forces.

In addition is important to visualize the flow around the wing, the following figures represent 3D air flow around the wing.

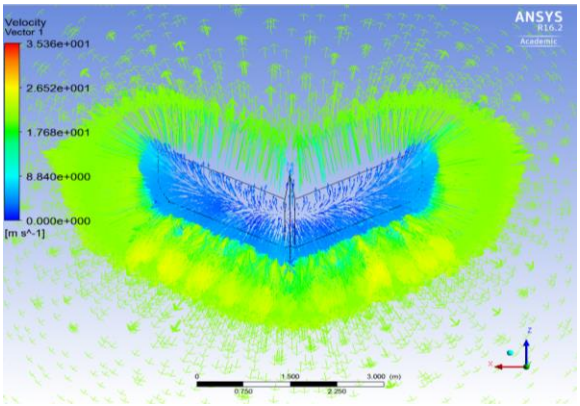

(a)

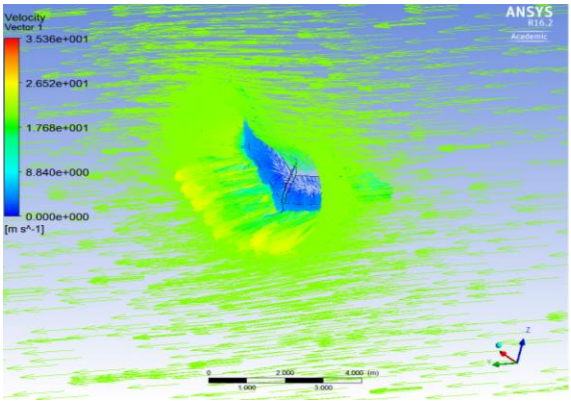

(b)

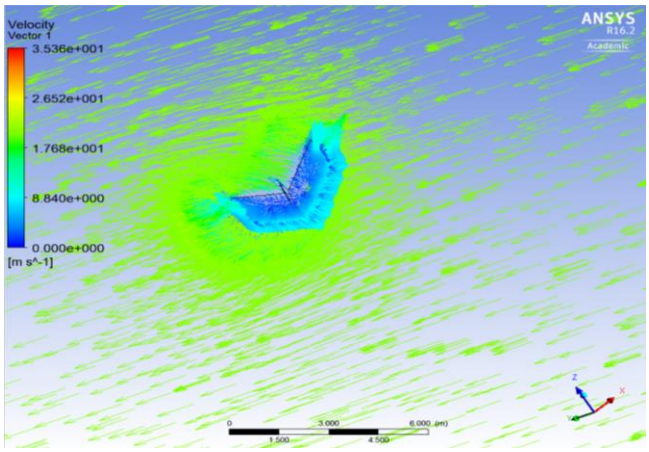

(c)

Figure 19: a, b, c) Kite-Wing subject to a normal airflow of 20 m/s

.

B- Stresses and deformations on Sailcloth

After finding the force applied by the air flow on the sail material, the next step was to assess the strength of frame under the force of the sail and the force of the user. In addition, the sail was simplified ,modeled and simulated in ANSYS as planar surface, because the 3D sail model takes too much time to simulate, it gives erroneous results and most of the time the results do not converge. In order to simulate the simplified wing version the following steps were taken into consideration.

- Geometry
- Meshing
- Physics Setup
- Numerical Results

1- Geometry

To start with, the sail was modeled with the same dimensions of the actual wing, as a surface area with and figure illustrates it. Afterwards, the static structural module was opened, and the thickness of the sail was defined as 0.001 m.

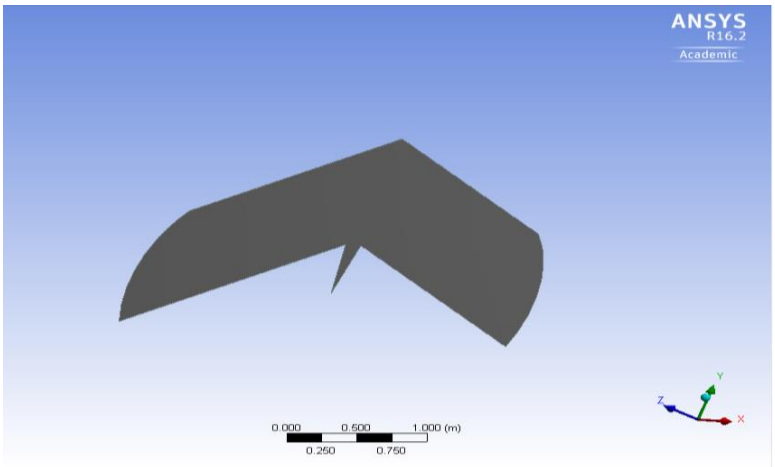

Figure 20: Simplified Sail model.

2- Mesh

The mesh was set to fine relevance center and with a minimum size element of 0.05 m as figure shows

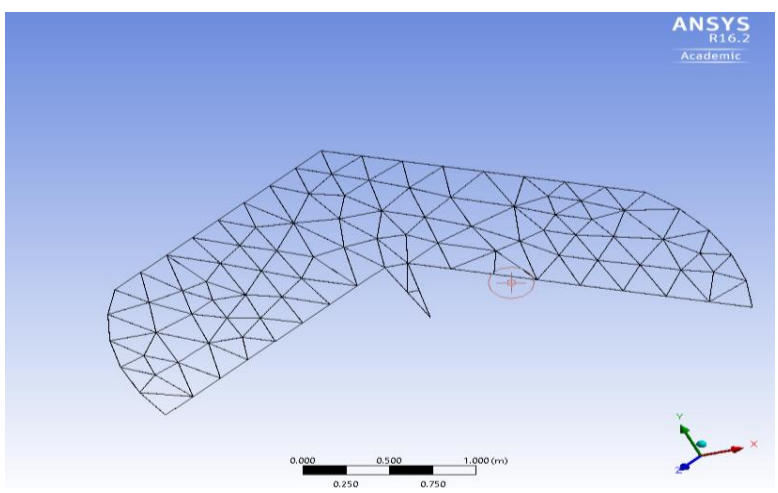

Figure21: Meshing of the simplified sail version

3- Physics Setup

In material that was assigned to the sail is PET (Polyethylene terephthalate) which is used a sailcloth in many applications, and it has the following mechanical properties.

Material	Young's modulus	Tensile strength	Poisson ratio
PET sailcloth	3100 MPa	1.35 g/cm^3	0.4

Table 7: Mechanical properties of PET (Polyethylene terephthalate)

In addition, the simplified sail was fixed from 4 edges and subjected a pressure of 275 Pa, and figure illustrates.

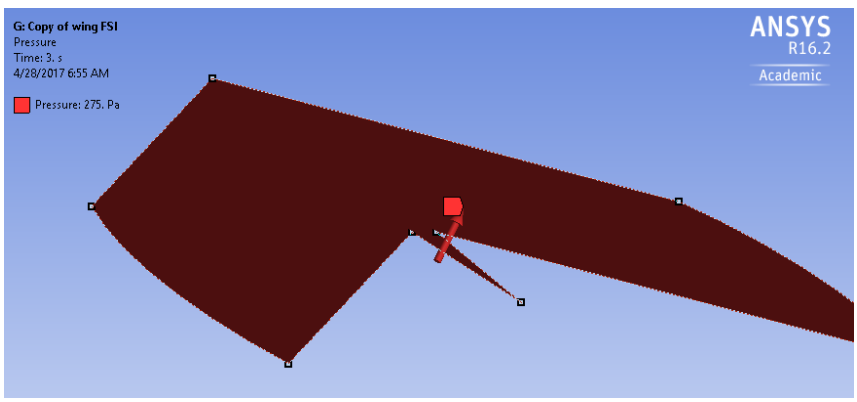

Figure 22: Pressure normal to the simplified wing surface.

4- Numerical Results

a- Deformation of the sailcloth

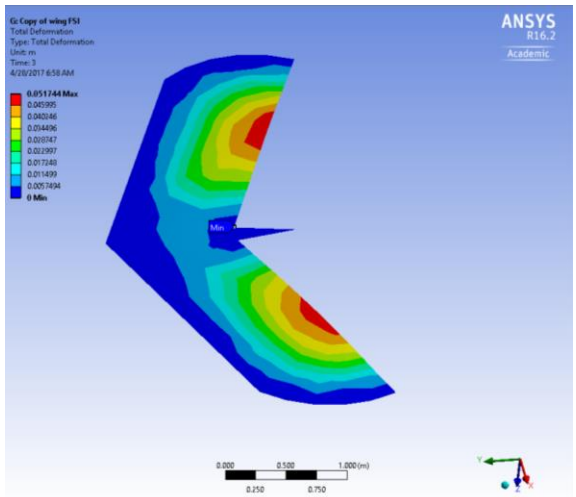

Figure 23: Sail deformation

Figure 24 shows that the maximum deflection which is 5.1 cm happens where the sailcloth is not fixed

b- Stresses on the sail cloth

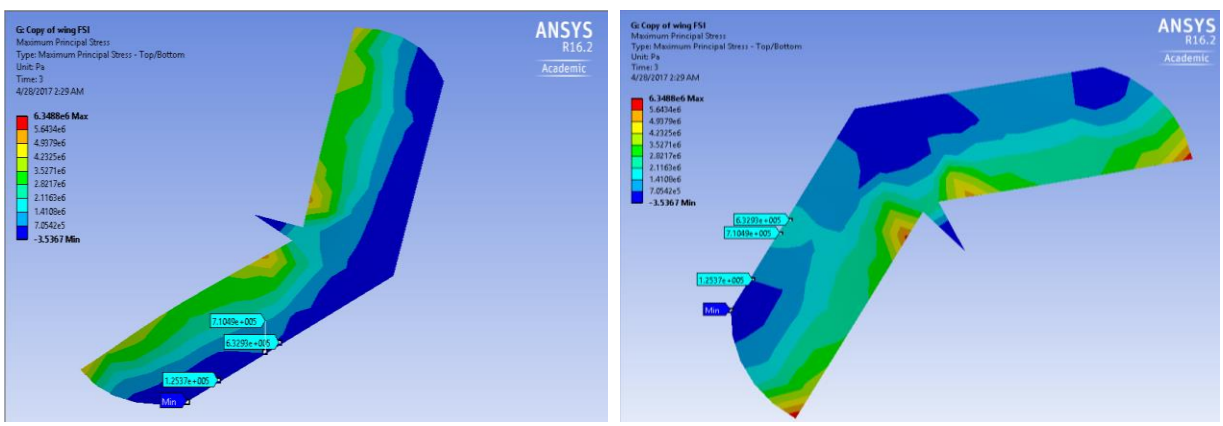

(a) (b)

Figure 24: a) Top view of the simplified wing b) Bottom view of the simplified wing

In figure 25, it is desired to find the maximum principle stress next the wing and near the leading edge, and its value 7.10 e5 Pa. Hence the force is: $F = \sigma * A = 7.10\ e5 * 0.001 * 1 = 700\ N$.

Where

A: Area in contact with the leading edge (m^2)

σ: Maximum principle stress (Pa)

F: Force (N)

C- Strength of the Kite-Wing's frame

The next step is to assess the strength of material under the force exerted by the sail and the one exerted by the user.

- Problem statement
- Geometry
- Physics Setup

1- Problem statement

The purpose from this structural analysis is to determine whether the frame of the Kite-wing can resist the forces applied by the sail material and by the user under a specific scenario. This scenario is about a user who is using the kite-wing when the wind velocity is 20 m/s where the wind is normal to the wing. This implies that the primary force that moves the user is the drag force.

2- Geometry

To start with, the frame is made of 6 cylindrical tubes, 7 connectors, and many bolts and nuts. These components were modeled in CAD software ANSYS. And the dimensions of all the Kite-Wing's components are provided in the following figures:

a- Connectors

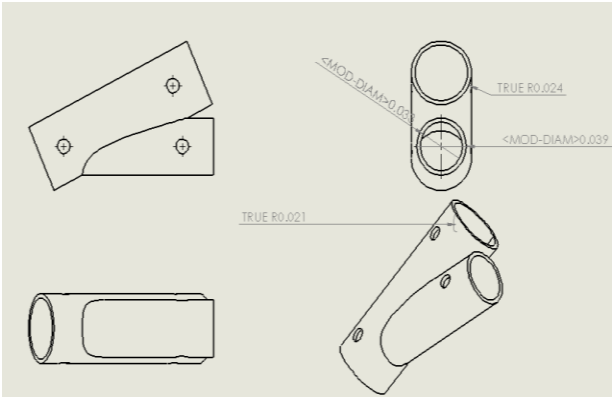

(a)

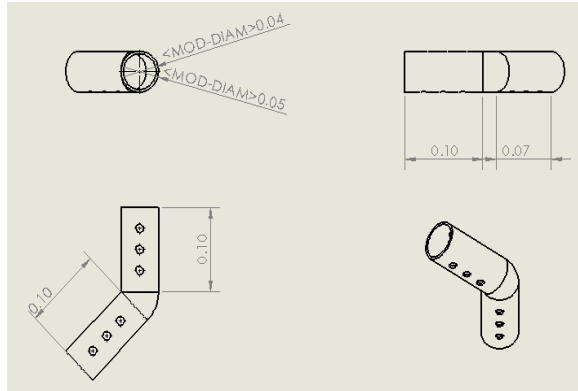

(b)

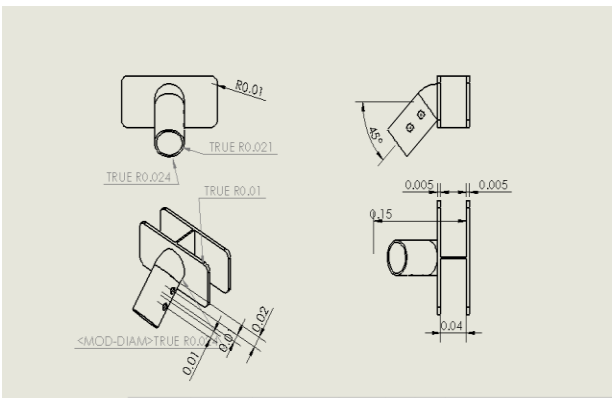

(c)

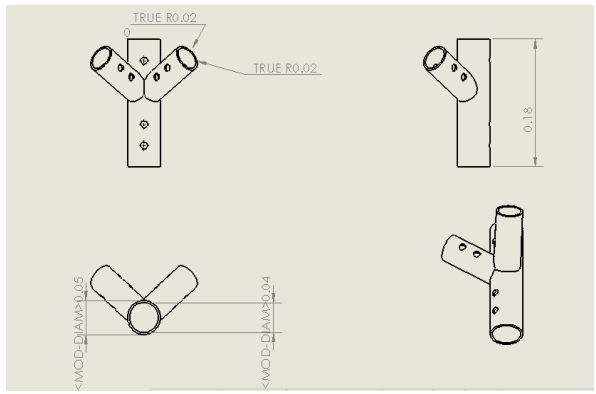

(d)

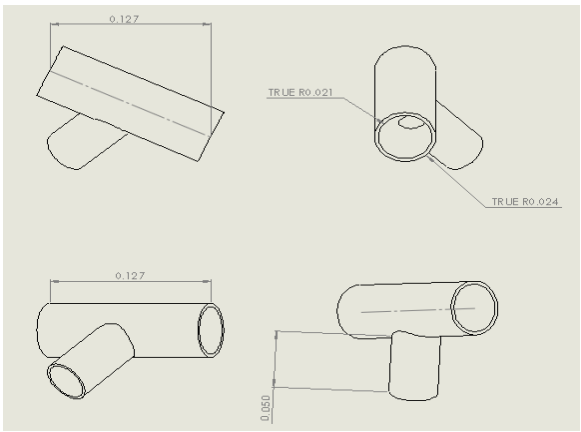

(e)

Figure 25: Dimensions of the connectors a, b, c, d

b- Cylindrical tubes

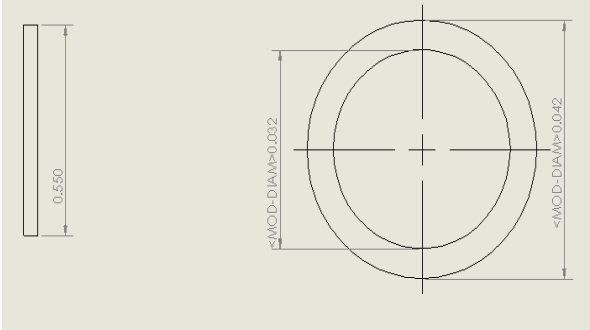

(a)

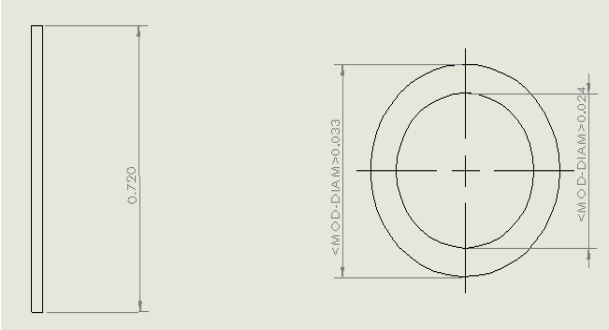

(b)

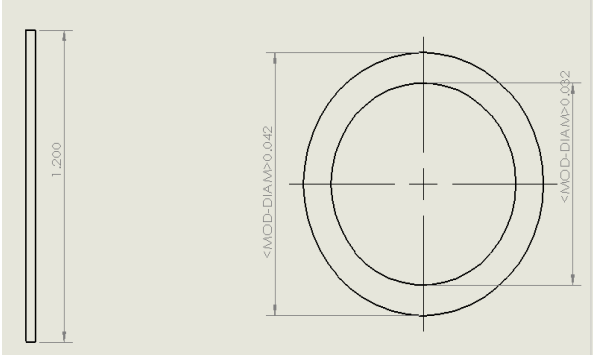

(c)

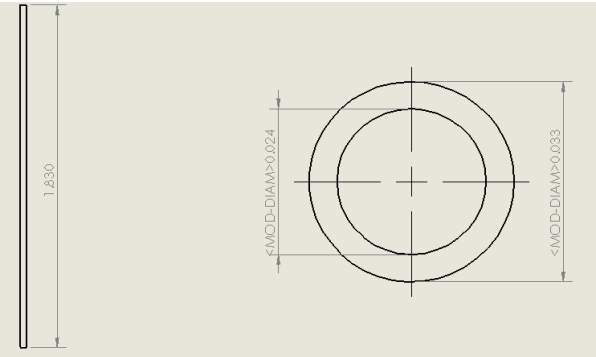

(d)

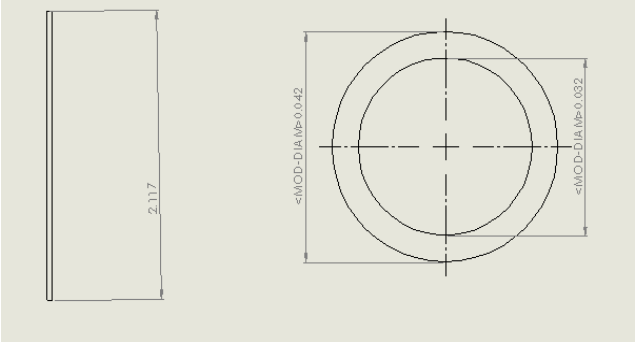

(e)

Figure 25: a, b, c, d, e) Cylindrical tubes with different dimensions.

c- Bolts and nuts

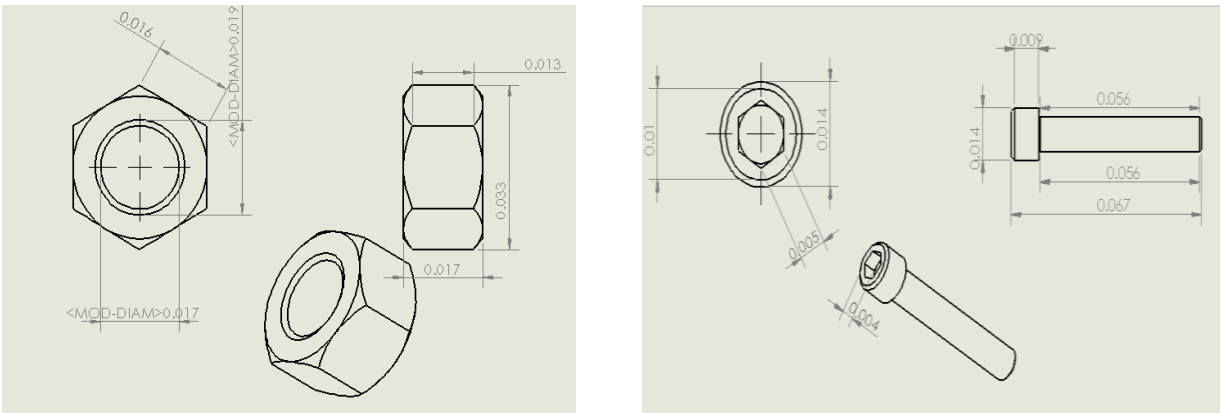

(a) (b)

Figure 26: a) Dimensions of hexagonal nut b) Dimensions of the bolts

d- Assembly of the frame

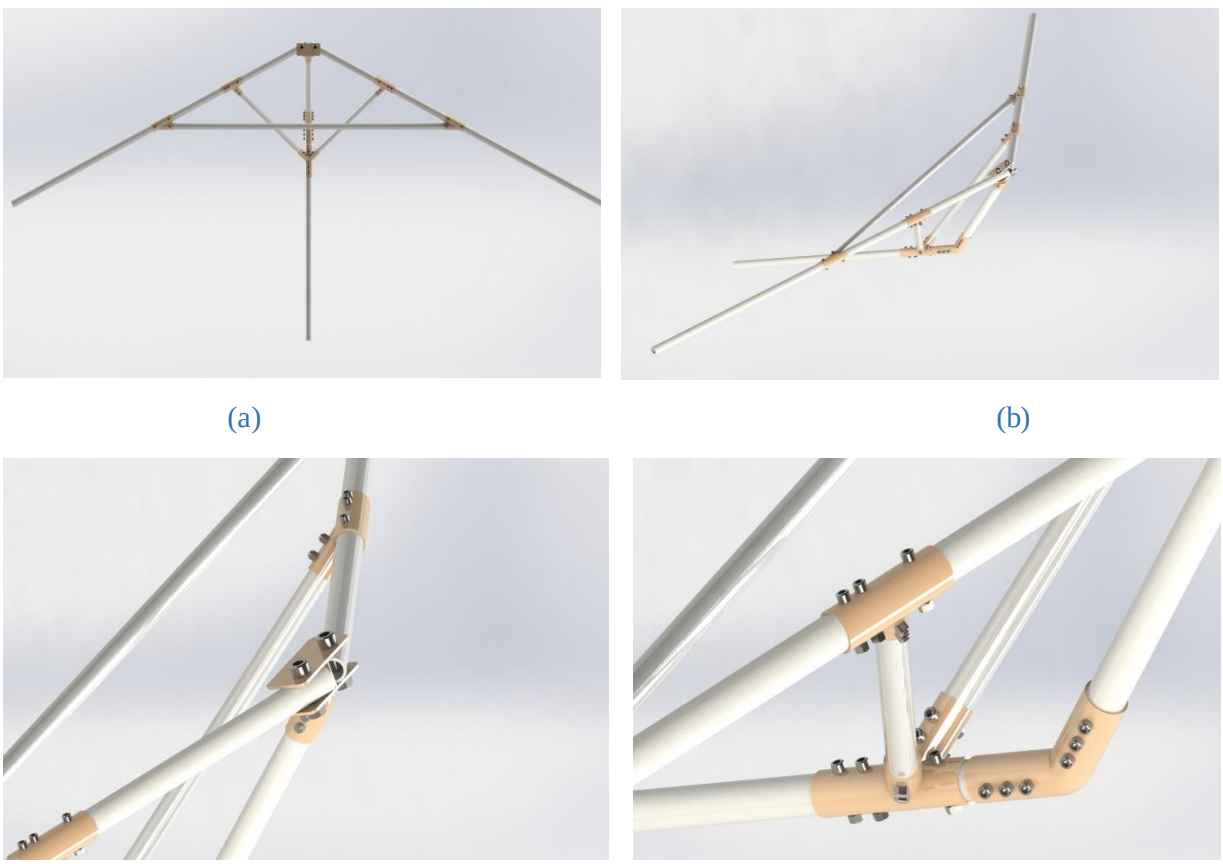

(a) (b)

(c) (d)

Figure 27: a) Top view of the frame b) Side view of the frame c) First example connections d) Second example of connections

3- Physics setup & Solution

Components	Bolts and nuts	Cylindrical tubes	Connectors
Materials	Mid carbon steel	Aluminum 6000	HDPE
Elastic Modulus	2090405.5 Kgf/cm^2	24575.01 Kgf/cm^2	3846.35 Kgf/cm^2
Poisson ratio	0.29	0.38	0.41
Density	0.00785 Kgf/cm^3	0.0013 Kgf/cm^3	0.002 Kgf/cm^3

Table 8: Material assignment and material mechanical properties

The appropriate materials were chosen based the 700 N sail force on the frame. And it is worth mentioning that in the Kite-Wing's frame there is a 1.1 m cylindrical tube which is free to move and fixed next to the connector as encircled in figure

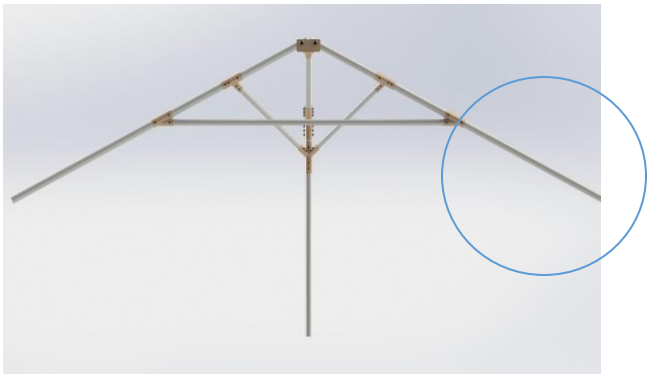

Figure 28: Free - end member

This tube was treated as a cantilever under a distributed load, hence, the following equation was used in order to determine the maximum stress that this considered to part of the Kite-Wing $\sigma = Wl^2/2Z$ and $Z = \left(0.78(Ro^4 - Ri^4)\right)/Ro$.

Where

W: load (N)

L: length (m)

Ro: Outer radius (m)

Ri: inner radius (m)

The load is 700 N and the dimensions of the tube are Ro = 0.021m, Ri =0.016m, and l =1.1 m. And after plugging these values the stress is $\sigma = 92.60MPa$. Also, since this value is less than tensile yield strength (105 MPa) of Aluminum 6005-T1 series the material is considered to be a good candidate.

IV- Conclusion

Last but not least, in this project an attempt to analyze the Kite-Wing holistically. This involved a study of aerodynamics and structural mechanics using hand calculations, computational fluid dynamics, and finite element method. The Kite-Wing performance was assessed using CFD simulations, and it was found that the wing has good aerodynamic properties, such as, the high lift coefficients and lift force that is enough to thrust the user forward. Also, the strength of the frame material was assessed and it was found that Aluminum 6000 series is a good candidate, since it has a good strength to weight ratio.

Although this project dealt with many important aspects of the Kite-Wing there are still other important details to tackle, for instance, the effect of the aero-elastic sailcloth on the flow and the effect of battens that are incorporated in the sailcloth.

V- Future Work

There are many levels at which the Kite-Wing can be improved. For example, the drag force could be decreased by reducing the camber of the airfoil that was chosen, since less turbulences will be gathered around under the wing. Moreover, improvement at the level of materials is also possible, meaning, that the kite wing can be made lighter, stronger and cheaper if appropriate material is chosen. Also, a study of that include aero-elastic properties of the sail will be dealt with, since sail material has effect on the flow which will certainly change the aerodynamic properties of the wing. And a more in depth structural analysis will be performed, especially, at the level of contacts between the tubes and bolts.

References

1. PBS, April 2008, http://www.pbs.org/wgbh/nova/spiesfly/uavs.html

2. NASA Report: “A Report Overview of the Civil UAV Capability Assesment.”

3. Mueller, T.J., Fixed and Flapping Wing Aerodynamics for Micro Air Vehicle Applications. Reston, VA: AIAA, 2001.

4. Grauer, J., and Hubbard Jr., J.E. “Development of a Sensor Suite for a FlappingWing UAV Platform,” AIAA Paper No. 2008-224, 46th AIAA Aerospace Sciences Meeting and Exhibit, Reno, NV January 7-10, 2008.

5. Hein, B., Chopra, I., "Hover Performance of Micro Air Vehicles: Rotors at Low Re," American Helicopter Society International Specialists Meeting on Unmanned Rotorcraft, Chandler, AZ, January 2005.

6. Bohorquez, F., Pines, D., "Rotor and Airfoil Design for Efficient Rotary Wing Micro Air Vehicles," 61st Annual American Helicopter Society Forum, Grapevine, TX, June 2005.

7. Ornithopter Zone, Aprill 2008,

8. Videler, J.V., Avian Flight. Oxford University Press, New York City, NY, 2005.

9. Shyy, W., Lian, Y., Tang, J., Viieru, D., Liu, H., Aerodynamics of Low Reynolds Number Flyers. Cambridge University Press, New York, NY, 2008.

10. Azuma, A. The Biokinetics of Flying and Swimming (2nd Ed). Reston, VA: American Institute of Aeronautics and Astronautics.

11. Ward-Smith, A.J., Biophysical Aerodynamics and the Natural Environment. John Wiley & Sons, New York, 1984. 216

12. Dr. James E. Hubbard Jr., Morpheus Laboratory Director, National Institute of Aerospace, 100 Exploration Way, Hampton, VA, 23666. Ph: 757-325-6830.

13. Anders, J.B., "Biomimetic Flow Control," AIAA Paper No. 2000-2543, Fluids 2000 Conference and Exhibit, Denver, CO June 19-22, 2000.

14. Shyy, W., Berg, M., and Ljungqvist, D., "Flapping and flexible wings for biological and micro air vehicles," Progress in Aerospace Sciences, Vol. 35, 1999, pp. 455-505.

15. Lian, Y., Shyy, W., Viieru, D., Zhang, B., "Membrane wing aerodynamics for micro air vehicles," Progress in Aerospace Sciences, Vol. 39, 2003, pp. 425-465.

16. Smith, M.J.C., Wilkin P.J., Williams, M.H., "The advantages of an unsteady panel method in modeling the aerodynamic forces on rigid flapping wings," The Journal of Experimental Biology, Vol. 199, 1996, pp. 1073-1083.

17. DeLaurier, J.D., "An aerodynamic model for flapping wing flight," The Aeronautical Journal of the Royal Aeronautical Society, April 1993, pp. 125-130.

18. Singh, B., and Chopra, I., "Dynamics of Insect-Based Flapping Wings: Loads Validation," AIAA Paper No. 2006-1663, 14th AIAA Adapative Structures Conference, Newport, Rhode Island, May 1-4, 2006.

19. Betteridge, D.S., Archer, R.D., " A Study of the Mechanics of Flapping Wings," Aeronaut Quarterly, May 1974, pp. 129-142.

20. Theodorsen, T., "General Theory of Aerodynamic Instability and the Mechanism of Flutter," NACA Report No 496, 1949.

21. Garrick, I.E. "Propulsion of a Flapping and Oscillating Airfoil," NACA Report No 567, 1936.